GaN/AlGaN Nanocolumn Ultraviolet LED using Double-Layer Graphene as Substrate and Transparent Electrode

Ida Marie Høiaas[1,*], Andreas Liudi Mulyo[1,2,*], Per Erik Vullum[3], Dong-Chul Kim[1], Lyubomir Ahtapodov[1], Bjørn-Ove Fimland[1], Katsumi Kishino[2,4,#] and Helge Weman[1,#]

* I.M.H. and A.L.M. contributed equally to this study.

[#] Corresponding authors: kishino@sophia.ac.jp, helge.weman@ntnu.no

[1] Department of Electronic Systems, Norwegian University of Science and Technology (NTNU), NO-7491 Trondheim, Norway
[2] Department of Engineering and Applied Sciences, Sophia University, 102-8554 Tokyo, Japan
[3] SINTEF Industry, NO-7465 Trondheim, Norway
[4] Sophia Nanotechnology Research Center, Sophia University, 102-8554, Tokyo, Japan

Abstract

The many outstanding properties of graphene have impressed and intrigued scientists for the last few decades. Its transparency to light of all wavelengths combined with a low sheet resistance makes it a promising electrode material for novel optoelectronics. So far, no one has utilized graphene as both the substrate and transparent electrode of a functional optoelectronic device. Here, we demonstrate the use of double-layer graphene as a growth substrate and transparent conductive electrode for an ultraviolet light-emitting diode in a flip-chip configuration, where GaN/AlGaN nanocolumns are grown as the light emitting structure using plasma-assisted molecular beam epitaxy. Although the sheet resistance is increased after nanocolumn growth compared with pristine double-layer graphene, our experiments show that the double-layer graphene functions adequately as an electrode. The GaN/AlGaN nanocolumns are found to exhibit a high crystal quality with no observable defects or stacking faults. Room temperature electroluminescence measurements show a GaN related near bandgap emission peak at 365 nm and no defect-related yellow emission.

KEYWORDS: graphene, semiconductor nanocolumn, UV optoelectronics, LED, nitride-based devices, electrical injection

With the emergence of new semiconductor nanomaterials and heterostructures, new possibilities for optoelectronics arise. The semiconductor materials most commonly used for optoelectronics today, like Si[1], GaAs, InAs[2], ZnO[3] and GaN with its alloys[2], exhibit structural imperfections when grown as heteroepitaxial thin-films, for instance twinning defects, threading dislocations and stacking faults. This is due to a large lattice mismatch between these materials as well as with conventional substrates. By nanostructuring the semiconductor materials in the forms of columns or pyramids, new combinations of materials can be explored, and new substrates can be employed for the epitaxial growth.

An intriguing potential substrate for epitaxial growth of semiconductors is graphene, the single-layer form of carbon, as it can not only act as an atomically thin crystalline growth template, but also has outstanding functional properties when it comes to strength, flexibility, electron and thermal conductivity[4,5]. Hybrid systems based on the growth of semiconductor nanocolumns on different graphitic substrates have been intensively studied in the last decade, with the aim of developing new functionalities and higher efficiency optoelectronic devices as for example solar cells, photodetectors, light emitting diodes (LEDs) and lasers. Such hybrid systems have been demonstrated for GaAs[6], InAs[7–9], InAsSb[10], In(Ga)As[11,12], ZnO[13,14] and GaN. With regards to the growth of GaN nanocolumns, different graphitic forms have been used as growth substrate, for instance graphite[15], transferred CVD graphene (single- and multilayer)[16–25] and epitaxial graphene[26]. However, these studies mostly focused on the growth of the nanocolumns, without further demonstration of a hybrid device realization.

In addition to the attributes already mentioned, graphene has the attractive property of being transparent in all parts of the electromagnetic spectrum and has been demonstrated as a top-emitting transparent conductive electrode (TCE) for GaN[27,28] and InGaN LEDs[29–31]. In contrast to the traditional TCE in optoelectronic devices, indium tin oxide, graphene is transparent in the whole UV region of the electromagnetic spectrum (100 to 350 nm)[32], offering a potential solution for devices operating in this region.

Recently, our group showed GaN/AlGaN nanocolumn growth with a single-layer graphene substrate as the bottom electrode[25]. However, so far there has been no realization of utilizing graphene simultaneously as the growth substrate and the TCE of a semiconductor device. Here, we

demonstrate a UV-A LED using transferred double-layer graphene (DLG) both as the substrate for GaN/AlGaN nanocolumn growth and as the TCE in the processed device. Along with the reduced sheet resistance of DLG compared to single-layer graphene[33], it is expected that the additional top layer of graphene will protect the bottom layer of graphene from plasma nitridation damage during growth. The electric current is thus injected directly from the conducting DLG substrate in a *vertical* flip-chip device configuration, which can be advantageous when compared to traditional mesa LED structures with lateral current injection that suffer from current crowding[34–36].

Nanocolumn growth and structural characterization

In this work, we have grown catalyst-free, self-assembled $Al_xGa_{1-x}N$/GaN nanocolumn heterostructures on transferred DLG on amorphous silica glass by radio-frequency plasma-assisted molecular beam epitaxy (RF-PAMBE) under N-rich conditions (see Methods for the detailed information on the growth). The intended LED structure is shown schematically in Figure S1a in the Supplementary Information, where each nanocolumn is designed to consist of 40 nm n-AlN, 140 nm n-GaN, 550 nm n-$Al_{0.25}Ga_{0.75}N$, 27 nm undoped GaN, 200 nm p-$Al_{0.25}Ga_{0.75}N$ and 20 nm p-GaN. Here, we would like to emphasize that the length of each aforementioned segment is based on nominal values. In addition, the indicated Al and Ga compositions are nominal compositions, i.e. based on the ratio between the Al and Ga fluxes (see Table S1 in Supplementary Information). To verify these values, further transmission electron microscopy (TEM) investigations were carried out and will be discussed in the following paragraphs. A thin AlN buffer layer does not only serve as a nucleation site for n-GaN[17,23–25], but it also reduces damage to the graphene induced by impinging active N species generated by the RF plasma source[17,23–26,37] and in-plane strain generated by GaN nucleation[23,38]. To achieve even higher density of nanocolumns, the AlN deposition method is modified[25] from the migration enhanced epitaxy (MEE) technique which was utilized to obtain 1 μm long vertically aligned GaN nanocolumns on single-layer[23,24] and multi-layer graphene[17]. In addition, a higher probability of vertical growth of n-GaN nanocolumns on graphene was achieved, which is important for the subsequent vertical n-AlGaN nanocolumn growth[39,40].

Shown in Figure 1a-b are the top- and bird-view scanning electron microscopy (SEM) images of the self-assembled GaN/AlGaN nanocolumns grown on DLG. It can be seen that the nanocolumns coalesce with each other, forming an almost continuous film-like layer in the top part of the nanocolumns. The top-view SEM image from the center area of the sample (Figure 1a) shows that

the geometry of some of the uncoalesced nanocolumns exhibits near-perfect hexagonal morphology. In addition, there are a few small gaps (less than 50 nm) between some nanocolumns and their neighbors. From some of the nanocolumns with distinguished hexagonal cross-sectional geometrical shape, the average top diameter is found to be about 220 nm. Figure 1b shows a bird-view SEM image, indicating that the nanocolumns are highly dense and vertically oriented with respect to the graphene/glass substrate, as well as demonstrating a relatively uniform height distribution. Figure S1b in the Supplementary Information is a representative side-view SEM image of the grown GaN/AlGaN nanocolumns, where the average height, average bottom- and top-diameter of the grown nanocolumns, as derived from twenty SEM images, are found to be 1070, 35 and 220 nm, respectively. It is evident that the nanocolumn geometry exhibits a highly inverse-tapered structure due to the abrupt growth temperature reduction by 200 - 220 °C starting from the p-AlGaN segment, forming a champagne glass-like structure, similar to the work reported by Sekiguchi et al.[39]. As a result of the low growth temperature (675 – 695 °C), the nanocolumns tend to grow faster in the radial direction, causing the top part of the nanocolumns to coalesce with each other. Such coalesced nanocolumns are used in order to ensure a uniform and continuous metal contact to the top p-GaN segment in the subsequent LED processing, preventing discontinuous metal deposition on p-GaN as shown in previous work[25]. Furthermore, it can be deposited without the use of any insulating filler material between nanocolumns. The reasons for lowering the growth temperature during growth of the p-AlGaN and p-GaN segments of the device structure are explained in more detail in the Supplementary Information.

Detailed structural characterization was further carried out by TEM. Figure 1c shows a bright-field (BF) TEM overview image of the self-assembled GaN/AlGaN nanocolumns. All nanocolumns grow in the [0001]-direction, which was observed by electron diffraction for more than twenty nanocolumns and is exemplified in the diffraction pattern in Figure S2a in the Supplementary Information. This is consistent with previous reports of GaN nanocolumns grown on single-layer[16,18,23,24] and multi-layer graphene[17,26]. The darker contrast nanocolumns shown in Figure 1c are oriented with the electron beam parallel to the $[\bar{2}110]$-direction, i.e. they possess a very similar in-plane orientation. Tilting the sample to different in-plane orientations reveals several clusters of identically oriented nanocolumns on the µm-scale. Since the CVD DLG used as a substrate is polycrystalline, the observed preferred in-plane orientation of the nanocolumns is an indication that they adopt an epitaxial orientation related to the graphene lattice and thus follow the orientation of a particular graphene grain[6]. The DLG can be distinguished in Figure 1d as indicated by the red

arrows. The exact number of layers cannot be confirmed by this image, as the graphene layers are buckled and the two-dimensional image of the TEM lamella thus indicates more than two layers[23]. The nanocolumns exhibit a pure wurtzite crystal structure and no interfacial layer, which is identical with our observation in the growth of n-GaN nanocolumns on graphene using an MEE-AlN buffer layer[23] but different from n-GaN nanocolumns grown directly on silica glass[41]. No dislocations, stacking faults or other defects are found in the GaN- and AlGaN-nanocolumn segments. The AlN buffer layer, however, is found to have some dislocations and point defects. Using high-angle annular dark-field scanning TEM (HAADF STEM) to get a Z-contrast image of the nanocolumns in Figure 1c, the different segments of the GaN/AlGaN nanocolumns can be distinguished, as shown in Figure 1e.

The AlN buffer layer, seen in the base of the nanocolumns, tends to assemble as a continuous layer, although there are a few AlN islands as well. Short stems consisting of n-GaN are clearly visible below the n-AlGaN nanocolumn segments. A slight oscillation of the Ga/Al-ratio in the n-AlGaN segment is noticeable, forming a superlattice-like structure as is more evident in the HAADF STEM image in Figure 1f (the line scan can be seen in Figure S2b in the Supplementary Information). The main reason for such composition inhomogeneity could be kinetical[42]; as a consequence of a difference in sticking coefficients and diffusion lengths for Al and Ga adatoms as well as a competition between Al and Ga incorporation during the nanocolumn growth. This would be the case for both the direct impingement on the top of the nanocolumns and for diffusion along the nanocolumn sidewalls[42,43]. As the higher Al-content barriers in the superlattice-like structure in the n-AlGaN segment are only ~2-3 nm thick, it is unlikely that they will affect the electronic properties of the nanocolumns. From Figure S2c in the Supplementary Information, a higher Al-content nanocolumn shell-layer can be seen surrounding the AlGaN nanocolumn core, which might act as a self-passivation layer for the nanocolumn side facets. No intrinsic GaN segment is observed in the TEM images, which is likely caused by the complete desorption of this layer during the growth interruption needed to reduce the temperature for the subsequent p-AlGaN growth, as the Ga desorption rate is very high at these substrate temperatures[44]. The p-AlGaN segment and thin p-GaN contact layer grow highly inverse-tapered (as desired for the subsequent process of top contact metallization), indicating a switch from N-polar to Ga-polar growth mode (for improvement of p-type doping efficiency)[45], which is further evidenced by a switch from planar to inclined interfaces at the top of the nanocolumns.

The elemental composition of the different segments is estimated by combining X-ray electron dispersive spectroscopy (EDS) with electron energy loss spectroscopy (EELS), using the pure AlN and GaN layers at the bottom and top of the nanocolumns as references, respectively. The results shown in Figures 1g indicate that the n-AlGaN segment has a composition of 76% Al close to the p-n junction, while the p-AlGaN segment has a composition of 42% Al (more detailed in Figure S2c in the Supplementary Information). These values may have contributions from the Al-rich shell leading to an overestimation of the Al-content in the n- and p-AlGaN segments. However, most of the large deviation from the designed n- and p-AlGaN segment composition of 25% Al is most likely caused by the higher Ga desorption rate as explained above.

Graphene electrode

The nitrogen plasma sources utilized during RF-PAMBE growth of III-N nanocolumns are known to have a damaging effect to graphene[23–26,37]. To assess the extent of the possible damage, the DLG was characterized by micro-Raman spectroscopy and sheet resistance measurements before and after nanocolumn growth. Figure 2a shows the average micro-Raman spectrum from 1600 measurements of DLG before and after nanocolumn growth. The graphene is notably damaged after growth, as evidenced by the increase in the defect-related D-peak at ~1350 cm^{-1}, the reduction in the G- and 2D-peaks at ~1600 cm^{-1} and ~2700 cm^{-1} and the appearance of the D'-peak at ~1620 cm^{-1}. Mapping the peak intensity ratio of the D- and G-peaks in Figure 2b reveals that the defect distribution is non-uniform in graphene after the nanocolumn growth, with some areas resembling the pre-growth graphene quality while others are extensively damaged. The increased presence of defects in graphene may lead to an increase in carrier scattering and therefore an increase in the graphene sheet resistance. This is confirmed by van der Pauw measurements, where the sheet resistance is found to increase from 329 Ω/□ before nanocolumn growth to 2326 Ω/□ after growth for the DLG. For single-layer graphene the sheet resistance increases more severely, from 779 Ω/□ before nanocolumn growth to 9510 Ω/□ after growth. It is worth to mention that the nitrogen plasma emission during nanocolumn growth is two times higher than for our previous work[25] (see Table S1 in Supplementary Information), resulting in more defective graphene and consequently a larger sheet resistance, especially for the single-layer graphene. However, for the case of DLG, the limited increase in sheet resistance shows that the top layer of graphene protects the bottom layer and thus limits the extent of the damage in the bottom layer. The UV transparency of transferred DLG on silica glass is reduced by an additional ~3% compared to that of transferred single-layer graphene on the same substrate carrier, retaining a total transmission of more than 80%[46].

Table 1 shows the D, G and 2D peak positions, intensities and ratios of the micro-Raman spectroscopy mapping, and maps of these parameters can be found in Figure S3 in the Supplementary Information. The apparent blue-shift of the G- and 2D-peaks for the DLG could be due to doping and/or strain in graphene after the nanocolumn growth[47]. It is known that exposure to nitrogen plasma may n-type dope graphene[37]. Using the correlation analysis developed by Lee et al[48], one can untangle how much strain and doping contributes to the Raman shift, but as there is a notable occurrence of defects in the graphene after nanocolumn growth, it is not possible to conclude on the exact origin of the peak-shifts.

LED fabrication and electrical characterization

The graphene-nanocolumn LED devices were fabricated as shown schematically in Figure 3. After nanocolumn growth, Ti was removed from the backside by mechanical removal and etching the sample in a buffered oxide etch, where hydrofluoric acid dissolves the Ti (Figure 3a). Contact areas to the graphene and nanocolumns were defined by photolithography (Figure 3b), and the metal contacts were deposited by electron beam evaporation (Figure 3c). A Ni/Au metal stack of 50/100 nm thickness was used as a top contact to the thin-film like p-GaN surface layer of the nanocolumns. To avoid deposition on the graphene, the top contact metals were deposited at a ~30° angle with regards to the substrate plane. For the bottom metal contact to the graphene, 200 nm Au was used, which is known to give an ohmic contact to graphene with a low contact resistance[49]. In this configuration, light can be emitted through the transparent graphene/silica glass substrate of the sample as a flip-chip type device (Figure 3d), and the continuous graphene electrode allows for vertical current injection through the nanocolumns. Figure 4a shows an optical microscopy image of the LED device, with the graphene-Au contact at the top of the image and p-GaN nanocolumn-Ni/Au contact at the bottom. The LED devices have apertures of 75 or 150 μm diameter, and the distances between the top and bottom metal contacts were fixed at ~100 μm.

Figure 4b shows the current-voltage (I-V) curves measured for six different LED devices on the same sample, and Figure 4c shows the same data in a semi-logarithmic scale. The different curves are from devices with different LED apertures. Devices with the same size show similar diode characteristics, indicating uniform nanocolumn growth and junction formation. For the same bias voltage, one would expect a quadrupled current level for the device with a doubled diameter, but as the current only increases by a factor of ~2, it is evident that the injection current does not scale with the aperture area. This could be an effect of the defect generation in the graphene layers caused

by nanocolumn growth, which also causes a relatively large sheet resistance, as was discussed above. The turn-on voltage is found to be 7.7 V (by intersecting the semi-linear region of the I-V curve between 10 V and 12 V and the voltage axis), somewhat larger than expected for a GaN/AlGaN nanocolumn LED[50], but considering the high Al-content of the n-AlGaN and p-AlGaN layers a higher turn-on voltage is more reasonable. However, the high resistance of the device makes it difficult to define an exact turn-on voltage, as multiple semi-linear regions could possibly be used to find different intersections. In the semilog-plot in Figure 4c, two voltage regions can be distinguished. A less steep slope below ~3.5 V can be seen, and the current below this value is attributed to leakage due to acceptor level recombination and electron overshoot[51].

Using the elemental compositions measured by combined EDS and EELS for the $Al_xGa_{1-x}N$ segments, the band gaps can be calculated by a model using local density approximation (LDA-1/2)[52]. The band gap of AlN is 6.28 eV and GaN 3.44 eV, so using a bowing parameter of 0.8 eV yields band gaps of 5.45 eV (227 nm) and 4.44 eV (279 nm) for the n-$Al_{0.76}Ga_{0.24}N$ and p-$Al_{0.42}Ga_{0.58}N$ segments, respectively[52]. The higher Al-composition at the n-doped side will increase electron leakage to the p-AlGaN side of the p-n junction.

LED emission and optical power output

Low temperature (LT) photoluminescence (PL) measurements show a main emission peak at 360 nm (3.44 eV), in addition to two weaker and less defined bands at 368 nm (3.37 eV) and 382 nm (3.25 eV), as shown in Figure 5. The latter band, typically referred to as the blue luminescence band, originating from donor-acceptor-pair recombination, in conjunction with the absence of a yellow luminescence band, strongly indicates that the PL emission originates from the top p-type GaN nanocolumn layer. The main emission peak at 360 nm (365 nm at room temperature (RT)) is most likely attributable to Mg_{Ga} acceptor bound excitons, as commonly done in the literature[53]. The internal quantum efficiency (IQE) at RT is estimated from the ratio of the integrated PL intensity at RT to the interpolated value at T = 0 K (see Figure S4 in Supplementary Information for further details). The obtained IQE is dependent on the excitation power density used[54], and the maximum value determined in our experiments was ~46 % at an excitation power of 5.5 mW.

The LED device performance was further investigated by RT continuous current injection electroluminescence (EL) measurements, where the EL is detected either by a UV sensitive detector inside an integrating sphere for power measurements, or a spectrometer for spectral information. Figure 6a-b shows the measured light under different current injection conditions,

with a main peak emission at 365 nm with a full width at half maximum (FWHM) of 37 nm at 20 V, which is slightly broader than near-UV GaN/AlGaN nanocolumn LEDs grown on Si substrates[55]. As already discussed above in relation with the TEM images in Figures 1e and 1g, there is no intrinsic GaN layer observed between the n-$Al_{0.76}Ga_{0.24}N$ and p-$Al_{0.42}Ga_{0.58}N$ nanocolumn segments. In addition, the main EL emission measured at 365 nm resembles closely the main PL emission band at RT, with the exception of the weak UV and blue-luminescence defect-related PL bands and a shorter-wavelength shoulder in the EL spectra appearing at high forward bias, as illustrated in Figure 6c. Therefore, it is most likely that similarly to the PL recombination, the EL recombination also occurs in the p-GaN nanocolumn layer. Several peaks contribute to the EL emission around 365 nm, indicating some local inhomogeneity in the thin p-GaN nanocolumn contact layer. There is no notable EL peak shift with increasing injection currents up to 1.1 mA. EL emission is detected from ~4.5 V, and the intensity is seen to increase linearly with the injected current at lower voltages before saturating at higher voltages > 18 V. No defect-related yellow EL emission was detected[56], as evidenced by the semi-logarithmic data representation of the inset in Figure 6a.

The external quantum efficiency (EQE) of the LED is a product of the IQE, the current injection efficiency (CIE) and the light extraction efficiency (LEE). Figure 6d shows the measured optical power with respect to the injected current. The slope of the dependence gradually decreases as the current increases due to droop[57], which can be more clearly seen by calculating the EQE as a function of injection current. The EQE is defined as the ratio of emitted photons over the number of injected electrons as given by the expression

$$EQE = \frac{q * P_{opt}}{I * h\nu} \quad (3)$$

where q is the electron charge, P_{opt} is the measured optical power, I is the injected current and $h\nu$ is the energy of the emitted photons. The measured EQE is shown in Figure 6e, and it is clear that the LED device is most efficient at current injections around 0.05 mA for a 150 μm diameter aperture device, with a continuous decrease in the EQE with increasing forward bias. A major factor for the low EQE of this LED is believed to be the low effective hole doping in especially the p-AlGaN segment causing hole-blocking at the p-GaN/p-AlGaN interface. Due to this the holes cannot reach the middle of the p-n junction and instead the EL recombination occurs in the thin p-GaN contact layer which is intrinsically a region with a low EQE. The absorption of the 140 nm

long n-GaN segment at the emission wavelength of 365 nm can be considered to be negligible. However, one must design a shorter n-GaN segment for UV LEDs emitting below 365 nm as the absorption coefficient increases abruptly above the GaN band gap[58]. In this study, the nanocolumns are randomly positioned (by self-assembly) across the graphene substrate. However, controlling the nanocolumn diameter and spacing by e.g. selective area growth with a hole-patterned mask can potentially increase the EQE by enabling coupling of the light emission into guided modes along the nanocolumns, as demonstrated in AlGaN- and InGaN-based nanocolumn/nanopyramid arrays[50,59–62]. Furthermore, one can reduce EQE droop by inserting an electron blocking layer on the p-side of the active layer, preventing electrons from overshooting the recombination region[63]. By incorporating quantum wells in the active layers, the efficiency can be further improved as the probability of radiative recombination increases[64]. Reducing the sheet resistance of graphene would lower the operating voltage of the LED, and there are several methods to achieve this. The reduction of plasma-damage has already been discussed, but in addition conducting elements can be deposited on the graphene if the LED is delaminated from the glass substrate[65]. Examples of conducting elements are Ag nanowires[66] and Au dots[67].

To summarize and conclude, we have shown that DLG can be used as a substrate for RF-PAMBE growth of GaN/AlGaN nanocolumns, and subsequently as the transparent electrode in a fabricated UV-A LED device. Although graphene gets damaged by plasma-activated nitrogen during the nanocolumn RF-PAMBE growth, the DLG retains its prominent characteristics and functions as a transparent electrode. Electroluminescence emission is achieved during continuous biasing at a wavelength of 365 nm with no defect-related yellow emission. Based on temperature dependent PL an IQE of ~46 % is estimated, confirming the high crystal quality of the nanocolumns. These results indicate that graphene can be used as a functional substrate and electrode for III-nitride-based device technology. Furthermore, we have indicated several possible steps for growth and device design optimization to improve the EQE, now that this platform has been established.

Figures

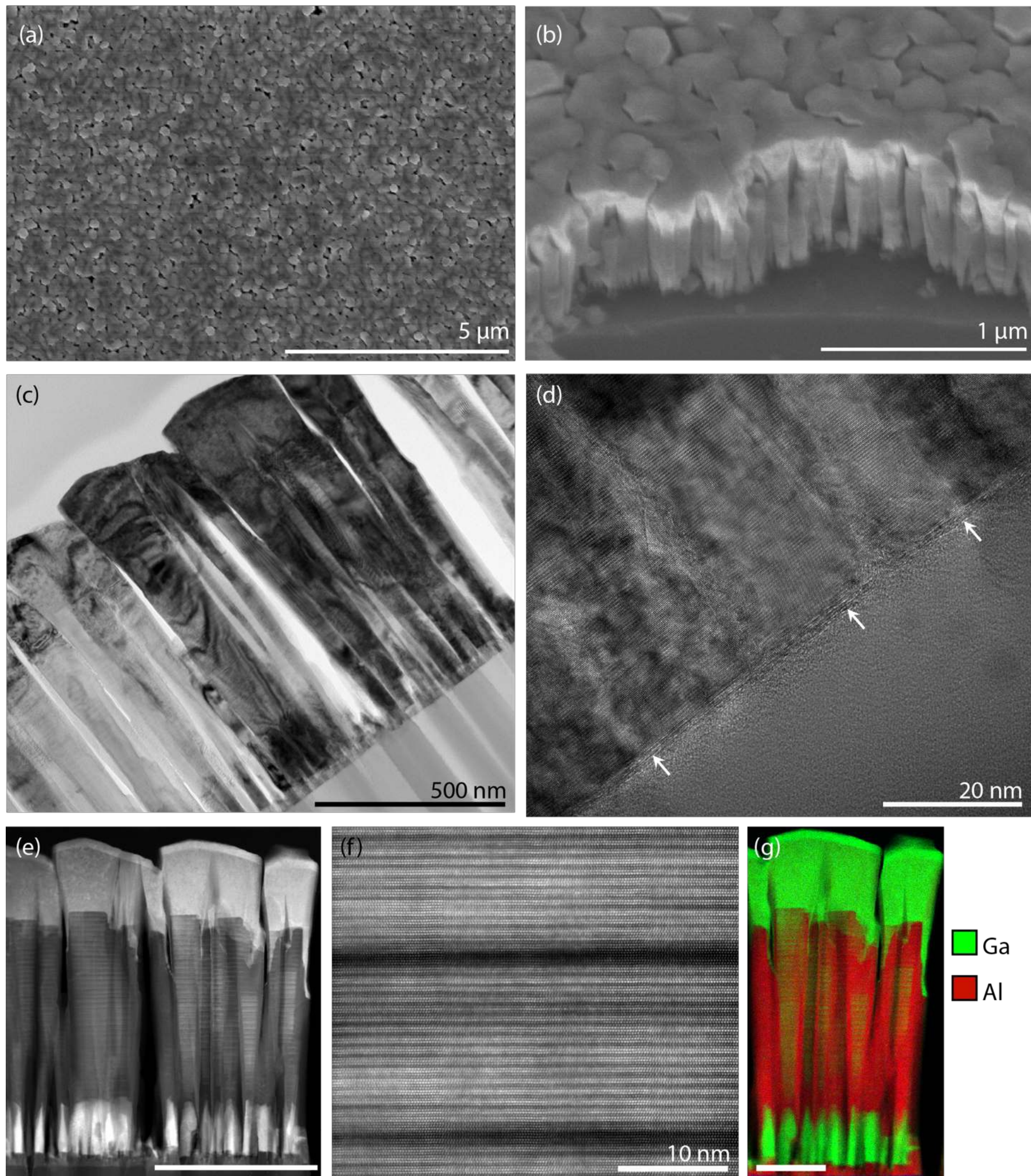

Figure 1. Overview of self-assembled GaN/AlGaN nanocolumns by SEM and their structural details by TEM. (a,b) Top- and bird-view SEM images of nanocolumns grown on DLG transferred onto amorphous silica glass. (c) BF TEM image of the nanocolumns shows local preferential

orientation as several neighboring nanocolumns are simultaneously on-axis, indicating epitaxy with the graphene substrate. The nanocolumns grow in the [0001]-direction. (d) High resolution BF TEM image showing the DLG (white arrows) between the amorphous silica glass support and the crystalline nanocolumns. (e) A superlattice-like structure can be observed by HAADF STEM (scale bar 500 nm). (f) High-resolution HAADF STEM image of alternating Al-rich/Ga-rich layers in the superlattice-like n-AlGaN nanocolumn segment. (g) Compositional mapping by EDS and EELS of the different GaN/AlGaN segments shows an actual nanocolumn heterostructure consisting of n-AlN/n-GaN/n-$Al_{0.76}Ga_{0.24}N$/p-$Al_{0.42}Ga_{0.58}N$/p-GaN (scale bar 200 nm).

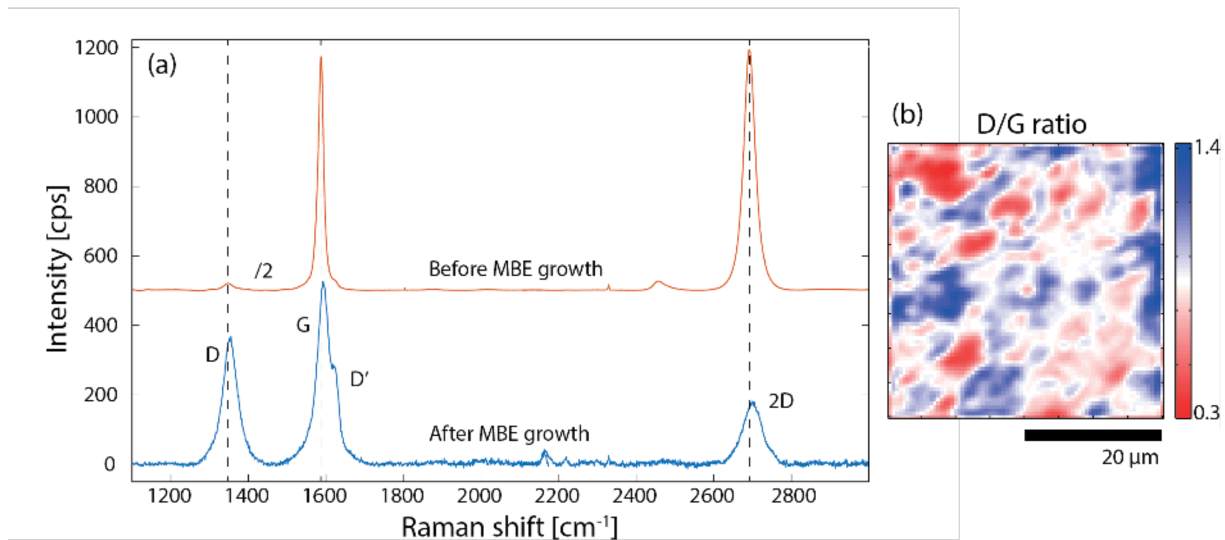

Figure 2. Micro-Raman characterization of DLG before and after RF-PAMBE GaN/AlGaN nanocolumn growth. (a) Averaged micro-Raman spectra from a 40x40 µm area with a 1 µm step size before (offset by 500 cps for clarity) and after nanocolumn growth, respectively. The intensity of the spectra taken before NC growth have been divided by two, and peak positions are indicated by the dashed lines. (b) Map of the same area shows the spatial variation of defects as represented by D/G peak intensity ratio.

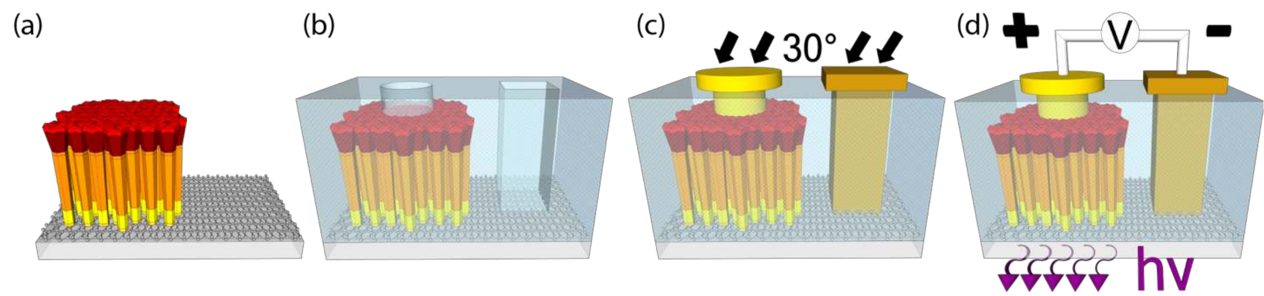

Figure 3. Schematic of the fabrication steps of the flip-chip UV LED device. (a) The nanocolumns are grown by RF-PAMBE on a DLG/silica glass substrate. (b) An insulating polymer is deposited and separate areas of graphene and nanocolumns are opened for the bottom and top metal contacts, respectively. (c) A Ni/Au metal stack contacts the top layer of p-GaN of the nanocolumns (deposited at an angle of 30°with the substrate plane), while Au contacts the graphene at the bottom. (d) The LED device is biased between the two contacts, and light is emitted through the graphene/silica glass substrate in a flip-chip configuration.

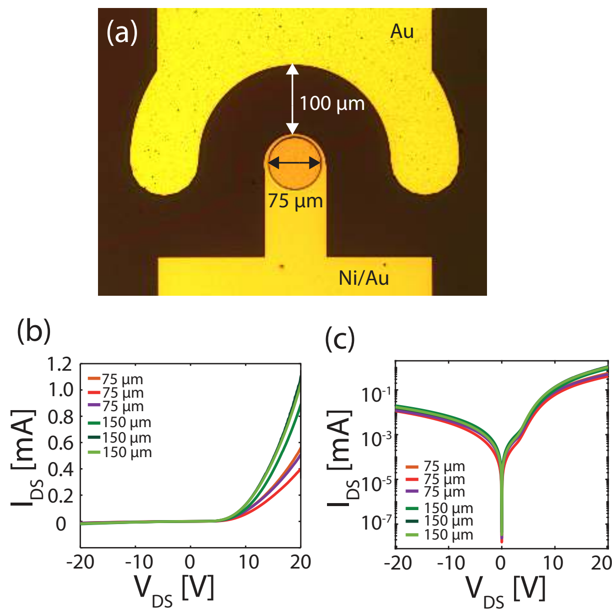

Figure 4. Processed LED device and I-V characteristics. (a) Optical microscope image from the p-GaN side of a 75 µm diameter aperture LED device (before flip-chip). (b,c) Linear and logarithmic I-V characteristics, respectively, from six LED devices with aperture sizes of 75 and 150 µm diameters.

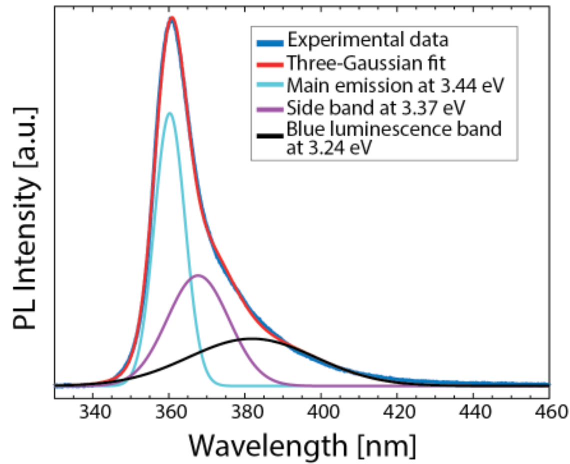

Figure 5. Low temperature 10 K photoluminescence spectrum of the LED device. The main PL emission is at 360 nm (3.44 eV), with two side bands at 368 nm (3.37 eV) and 382 nm (3.25 eV). For an interpretation of the PL spectrum see main text.

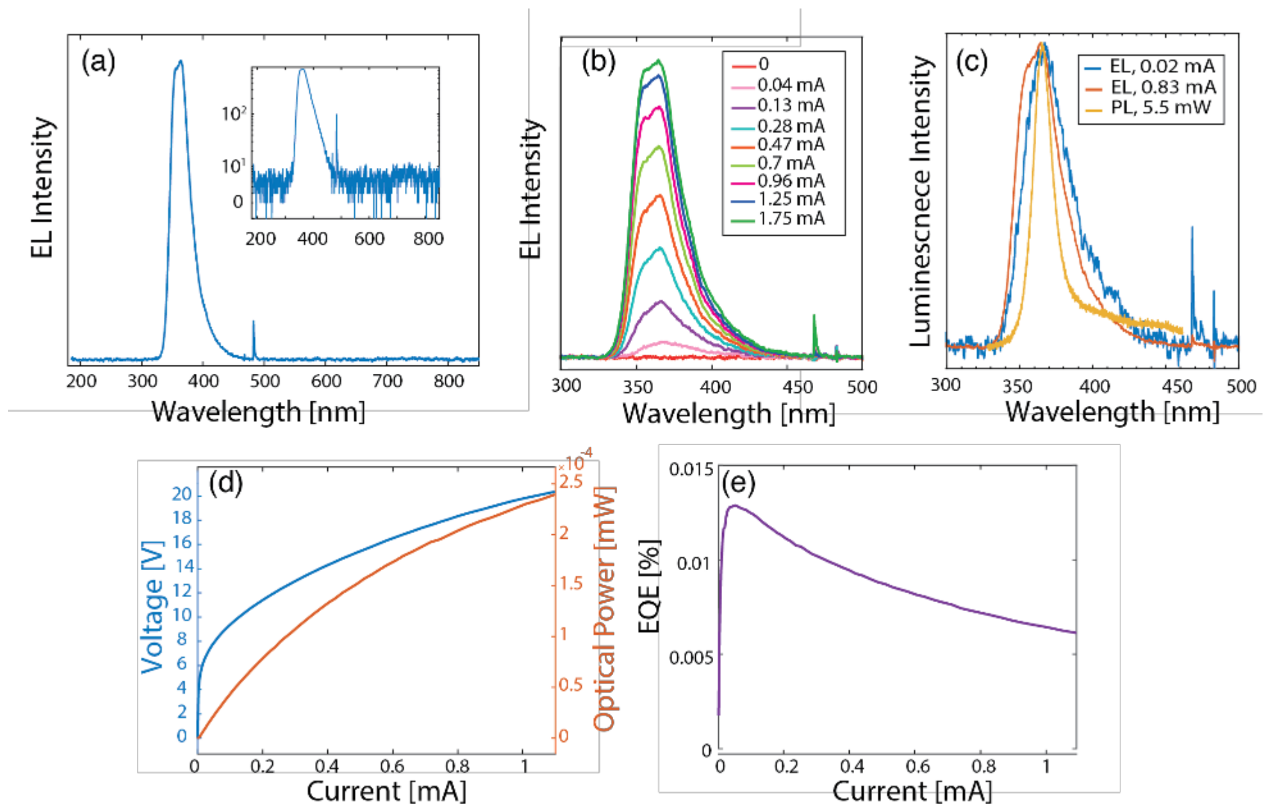

Figure 6. Room temperature electroluminescence measurements and LED device efficiency. (a) Electroluminescence spectrum measured for a 150 µm diameter aperture LED device under a bias of 20 V, with the logarithmic plot in the inset, showing a peak emission at 365 nm. (b) EL spectra at different injection currents. (c) Comparison between RT PL and EL spectra normalized to their

respective maximum intensity. (d) Voltage and optical output power dependency on injection current. (e) External quantum efficiency (EQE) at varying injection current measured using an integrating sphere.

Tables

Table 1. Micro-Raman peak positions, intensities and ratios.

Sample	Median D/G ratio	Median G		Median 2D			Median 2D/G ratio
		Position [cm^{-1}]	Intensity [cps]	Position [cm^{-1}]	Intensity [cps]	FWHM [cm^{-1}]	
DLG before MBE growth	0.04	1587	1003	2692	1314	37	1.31
DLG after MBE growth	0.9	1597	532	2698	169	58	0.32

Methods

Substrate preparation

The DLG is formed by two successive transfers of single-layer graphene. In this work, we used commercially available DLG as a substrate which was synthesized using chemical vapor deposition on Cu foil[33] and transferred to a substrate carrier of amorphous silica glass by Graphene Platform Corp. (Tokyo, Japan). The backside of the substrate was coated with an approximately 300 nm thick Ti layer for efficient and uniform absorption of thermal radiation from the heater to the substrate, as well as assisting the pyrometer reading during nanocolumn growth.

Growth of GaN/AlGaN nanocolumns

The catalyst-free and self-assembled GaN/$Al_xGa_{1-x}N$ nanocolumn heterostructures were grown in an EpiQuest RF-PAMBE system under N-rich conditions[17,39]. Standard effusion cells were used to supply Al, Ga, Mg (p-type dopant) and Si (n-type dopant) atoms, while atomic nitrogen was supplied from an RF plasma source operating at 450 W. Growth temperatures were recorded both from thermocouple readings near the Ti-coated backside of the silica glass substrate carrier and from pyrometer readings, in order to obtain as good as possible control over the substrate temperature. For the purpose of consistency, the growth temperatures stated hereafter refer to the pyrometer readings. The length/thickness for each segment/layer mentioned in the next paragraph

are nominal values based on the ratio between the Al and Ga fluxes (see Table S1 in Supplementary Information).

To start the nanocolumn growth, an Al seeding layer with Si atoms were deposited at 805 °C before the graphene substrate was exposed to N plasma. After that, the Si, Al and N shutters were opened simultaneously to form an n-AlN buffer layer with a thickness of approximately 40 nm[25]. Afterwards, a segment of about 140 nm[25] high n-GaN nanocolumn segments were formed at 895 °C, acting as a template for n-AlGaN[39], minimizing the chance of coalescence and/or quasi-film-like structures[40]. Subsequently, 550 nm long n-$Al_{0.25}Ga_{0.75}N$ nanocolumn segments were grown at 915 °C, followed by an active region of 27 nm thick intrinsic GaN segment grown at 895 °C. Radial nanocolumn development is anticipated, increasing the chance of achieving champagne-glass structure for the following nanocolumn segments[39]. Using this method, one can increase the diameter of nanocolumns and thus coverage without introducing a higher Al flux[25]. Next, a 200 nm thick p-$Al_{0.25}Ga_{0.75}N$ segment was grown at 695 °C, and finally, 20 nm thick p-GaN grown at 675 °C was used as a p-type contact layer. Each nanocolumn segment has its own distinctive growth condition with respect to Al, Ga, Si and Mg beam equivalent pressures, N_2 flow rate and growth time, as summarized in Table S1 in the Supplementary Information.

Micro-Raman measurements

A Renishaw inVia Reflex system with a 100 mW 532 nm laser, a 50x confocal objective and a spectral resolution of less than 1 cm^{-1} was used to map 40x40 µm areas on the samples. 10 mW laser power with a dwell time of 10 s was used for the acquisitions, and spectra shown in Figure 2a are averaged from 1600 individual measurements.

SEM imaging

Secondary electron images were taken with a Hitachi SU8000 system at an acceleration voltage of 5 kV.

TEM imaging

The cross-section TEM lamella was prepared by a FEI Helios G4 UX dual-beam FIB-SEM. Two protection layers of carbon, the first one made by e-beam assisted deposition and the second by ion-beam assisted deposition, were deposited on the surface of the selected area prior to milling. Coarse thinning was performed at 30 kV ion-beam acceleration voltage, while the final

thinning was performed at 5 and finally 2 kV to minimize Ga implantation and surface amorphization.
TEM characterization was performed with a double Cs-corrected cold-FEG JEOL ARM 200CF, operated at 200 kV and equipped with a 100 mm^2 (0.98 sr solid angle) Centurio SDD for X-ray energy dispersive spectroscopy (EDS) and a Quantum ER GIF for electron energy loss spectroscopy (EELS). In order to remove surficial hydrocarbons, the TEM lamella was gently plasma cleaned with a shielding holder 2 x 10 s prior to TEM characterization. Simultaneous EDS and dual-EELS were performed in scanning TEM (STEM) mode for chemical compositional analysis.

Electrical measurements

For van der Pauw measurements, Au contacts to graphene were made in the corners of a quadratic 0.5x0.5 cm^2 sample. The voltage was measured on opposite sides of the bias current path for both polarities to find the corresponding resistance, giving a total of eight measurements. These values were then inserted into the van der Pauw formula and the equation was solved for R_s numerically. The current-voltage measurements were done on a two-probe station connected to a Keithley 2636A sourcemeter.

Photoluminescence measurements

Continuous-wave (CW) excitation was achieved with a Kimmon Koha He-Cd laser operating at 325 nm. The excitation beam was focused on the sample using a 5 mm lens, achieving a spot size of ~ 0.42 mm. The sample was placed inside a Cryo Industries closed-cycle liquid He microscopy cryostat system equipped with a sample heater and thermometer for precise sample temperature control. PL detection was achieved with an Andor Shamrock 303i imaging spectrograph, using a 600 lines/mm grating blazed at 500 nm, dispersing the signal onto an Andor Newton electron multiplying charge-coupled device (EMCCD).

Electroluminescence spectral measurements

For LED electroluminescence measurements, a StellarNet EPP2000 UV-VIS (185nm - 850nm) compact spectrometer with a resolution between 0.4 nm (UV) and 0.25 nm (VIS), 2048 channels and a UV-transparent fiber was used.

Electroluminescence integrating sphere measurements

The integrating sphere measurement system consists of a 50 cm diameter integrating sphere ($BaSO_4$ coating) and a spectrometer consisting of a grating monochromator with step motor and photomultiplier tube. The optical resolution of the entire system is about 1.2 nm. According to the manufacturer, the minimum spectroradiometric accuracy of the system is +/-1% in the UVA and visible spectral region for each individual wavelength step. The LED sample is positioned in the center of the integrating sphere and contacted via contact probes. The LED samples are electrically driven and measured using a Keithley 2400 sourcemeter.

Acknowledgments

We acknowledge financial supports from the Research Council of Norway via the NANO2021 (259553) program and the Japan Society for the Promotion of Science KAKENHI (24000013). We would also like to acknowledge the Research Council of Norway for the support to the Micro and Nano-Fabrication Facility, NorFab (245963/F50). The TEM work was carried out on the NORTEM infrastructure (Grant No. 197405) TEM Gemini Centre, NTNU. We would like to thank Alain Ferber at SINTEF-Oslo, Michael Kneissl, Tim Wernicke and Martin Guttman of TU Berlin for their help in acquiring electroluminescence data. We are also indebted to Koji Yamano and Isamu Matsuyama of Sophia University for dedicated RF-PAMBE maintenance and insightful suggestions. Shunsuke Ishizawa, Yohei Nakagawa and Yuzo Matsui of Sophia University are appreciated for fruitful discussions.

Supplementary Information

Illustrative growth design diagram and additional SEM image (S1); detailed growth information (Table S1); explanation for using low growth temperature during p-type doping of nanocolumn structure; TEM analysis (S2); Raman measurements (S3); IQE measurements (S4).

References

(1) Soref, R. A. Silicon-Based Optoelectronics. *Proc. IEEE* **1993**, *81* (12), 1687–1706.

(2) Mokkapati, S.; Jagadish, C. III-V Compound SC for Optoelectronic Devices. *Mater. Today* **2009**, *12* (4), 22–32.

(3) Kozuka, Y.; Tsukazaki, A.; Kawasaki, M. Challenges and Opportunities of ZnO-Related

Single Crystalline Heterostructures. *Appl. Phys. Rev.* **2014**, *1*, 011303.

(4) Geim, A. K.; Novoselov, K. S. The Rise of Graphene. *Nat. Mater.* **2007**, *6*, 183–191.

(5) Balandin, A. A.; Ghosh, S.; Bao, W.; Calizo, I.; Teweldebrhan, D.; Miao, F.; Lau, C. N. Superior Thermal Conductivity of Single-Layer Graphene. *Nano Lett.* **2008**, *8* (3), 902–907.

(6) Munshi, A. M.; Dheeraj, D. L.; Fauske, V. T.; Kim, D. C.; Van Helvoort, A. T. J.; Fimland, B. O.; Weman, H. Vertically Aligned GaAs Nanowires on Graphite and Few-Layer Graphene: Generic Model and Epitaxial Growth. *Nano Lett.* **2012**, *12* (9), 4570–4576.

(7) Hong, Y. J.; Yang, J. W.; Lee, W. H.; Ruoff, R. S.; Kim, K. S.; Fukui, T. Van Der Waals Epitaxial Double Heterostructure: InAs/Single-Layer Graphene/InAs. *Adv. Mater.* **2013**, *25*, 6847–6853.

(8) Wallentin, J.; Kriegner, D.; Stangl, J.; Borgström, M. T. Au-Seeded Growth of Vertical and in-Plane III-V Nanowires on Graphite Substrates. *Nano Lett.* **2014**, *14*, 1707–1713.

(9) Anyebe, E. A.; Sandall, I.; Jin, Z. M.; Sanchez, A. M.; Rajpalke, M. K.; Veal, T. D.; Cao, Y. C.; Li, H. D.; Harvey, R.; Zhuang, Q. D. Optimization of Self-Catalyzed InAs Nanowires on Flexible Graphite for Photovoltaic Infrared Photodetectors. *Sci. Rep.* **2017**, *7*.

(10) Anyebe, E. A.; Sanchez, A. M.; Hindmarsh, S.; Chen, X.; Shao, J.; Rajpalke, M. K.; Veal, T. D.; Robinson, B. J.; Kolosov, O.; Anderson, F.; et al. Realization of Vertically Aligned, Ultrahigh Aspect Ratio InAsSb Nanowires on Graphite. *Nano Lett.* **2015**, *15* (7), 4348–4355.

(11) Mohseni, P. K.; Behnam, A.; Wood, J. D.; Zhao, X.; Yu, K. J.; Wang, N. C.; Rockett, A.; Rogers, J. a.; Lyding, J. W.; Pop, E.; et al. Monolithic III-V Nanowire Solar Cells on Graphene via Direct van Der Waals Epitaxy. *Adv. Mater.* **2014**, *26*, 3755–3760.

(12) Tchoe, Y.; Jo, J.; Kim, M.; Yi, G.-C. Catalyst-Free Growth of InAs/$In_xGa_{1-x}As$ Coaxial Nanorod Heterostructures on Graphene Layers Using Molecular Beam Epitaxy. *NPG Asia Mater.* **2015**, *7* (8), e206.

(13) Biroju, R. K.; Tilak, N.; Rajender, G.; Dhara, S.; Giri, P. K. Catalyst Free Growth of ZnO Nanowires on Graphene and Graphene Oxide and Its Enhanced Photoluminescence and Photoresponse. *Nanotechnology* **2015**, *26*, 145601.

(14) Lee, C. H.; Kim, Y. J.; Hong, Y. J.; Jeon, S. R.; Bae, S.; Hong, B. H.; Yi, G. C. Flexible Inorganic Nanostructure Light-Emitting Diodes Fabricated on Graphene Films. *Adv. Mater.* **2011**, *23*, 4614–4619.

(15) Nakagawa, S.; Tabata, T.; Honda, Y.; Yamaguchi, M.; Amano, H. GaN Nanowires Grown on a Graphite Substrate by Radio Frequency Molecular Beam Epitaxy. *Jpn. J. Appl. Phys.* **2013**, *52*, 08JE07.

(16) Heilmann, M.; Sarau, G.; Göbelt, M.; Latzel, M.; Sadhujan, S.; Tessarek, C.; Christiansen, S. Growth of GaN Micro- and Nanorods on Graphene Covered Sapphire: Enabling Conductivity to Semiconductor Nanostructures on Insulating Substrates. *Cryst. Growth Des.* **2015**, *15*, 2079–2086.

(17) Hayashi, H.; Konno, Y.; Kishino, K. Self-Organization of Dislocation-Free, High-Density, Vertically Aligned GaN Nanocolumns Involving InGaN Quantum Wells on Graphene/SiO_2 Covered with a Thin AlN Buffer Layer. *Nanotechnology* **2015**, *27* (5), 055302.

(18) Heilmann, M.; Munshi, A. M.; Sarau, G.; Göbelt, M.; Tessarek, C.; Fauske, V. T.; van Helvoort, A. T. J.; Yang, J.; Latzel, M.; Hoffmann, B.; et al. Vertically Oriented Growth of GaN Nanorods on Si Using Graphene as Atomically Thin Buffer Layer. *Nano Lett.* **2016**, *6*, 3524–3532.

(19) Ryu, S. R.; Ram, S. D. G.; Lee, S. J.; Cho, H.; Lee, S.; Kang, T. W.; Kwon, S.; Yang, W.; Shin, S.; Woo, Y. Vertical Current-Flow Enhancement via Fabrication of GaN Nanorod p-n Junction Diode on Graphene. *Appl. Surf. Sci.* **2015**, *347*, 793–798.

(20) Kang, S.; Mandal, A.; Park, J.-H.; Um, D.-Y.; Chu, J. H.; Kwon, S.-Y.; Lee, C.-R. Effects of Growth Temperatures on the Characteristics of N-GaN Nanorods–Graphene Hybrid Structures. *J. Alloys Compd.* **2015**, *644*, 808–813.

(21) Kumaresan, V.; Largeau, L.; Madouri, A.; Glas, F.; Zhang, H.; Oehler, F.; Cavanna, A.; Babichev, A.; Travers, L.; Gogneau, N.; et al. Epitaxy of GaN Nanowires on Graphene.

Nano Lett. **2016**, *16*, 4895–4902.

(22) Chung, K.; Beak, H.; Tchoe, Y.; Oh, H.; Yoo, H.; Kim, M.; Yi, G.-C. Growth and Characterizations of GaN Micro-Rods on Graphene Films for Flexible Light Emitting Diodes. *APL Mater.* **2014**, *2*, 092512.

(23) Liudi Mulyo, A.; Rajpalke, M. K.; Kuroe, H.; Vullum, P.-E.; Weman, H.; Fimland, B.-O.; Katsumi, K. Vertical GaN Nanocolumns Grown on Graphene Intermediated with a Thin AlN Buffer Layer. *Nanotechnology* **2018**, *30*, 015604.

(24) Liudi Mulyo, A. et al. The Influence of AlN Buffer Layer on the Growth of Self-Assembled GaN Nanocolumns on Graphene. *Unpublished*.

(25) Liudi Mulyo, A. et al. Utilization of Graphene as Substrate and Bottom Electrode for High-Density and Vertically-Aligned GaN/AlGaN Nanocolumns. *Unpublished*.

(26) Fernández-Garrido, S.; Ramsteiner, M.; Gao, G.; Galves, L. A.; Sharma, B.; Corfdir, P.; Calabrese, G.; Schiaber, Z. D. S.; Pfüller, C.; Trampert, A.; et al. Molecular Beam Epitaxy of GaN Nanowires on Epitaxial Graphene. *Nano Lett.* **2017**, *9*, 5213–5221.

(27) Kim, B.-J.; Lee, C.; Jung, Y.; Hyeon Baik, K.; Mastro, M. A.; Hite, J. K.; Eddy, C. R.; Kim, J. Large-Area Transparent Conductive Few-Layer Graphene Electrode in GaN-Based Ultra-Violet Light-Emitting Diodes. *Appl. Phys. Lett.* **2011**, *99*, 143101.

(28) Kim, B.-J.; Yang, G.; Kim, H.-Y.; Baik, K. H.; Mastro, M. A.; Hite, J. K.; Eddy, C. R.; Ren, F.; Pearton, S. J.; Kim, J. GaN-Based Ultraviolet Light-Emitting Diodes with AuCl3-Doped Graphene Electrodes. *Opt. Express* **2013**, *21* (23), 29025.

(29) Kang, J.; Li, Z.; Li, H.; Liu, Z.; Li, X.; Yi, X.; Ma, P.; Zhu, H.; Wang, G. Pyramid Array InGaN/GaN Core-Shell Light Emitting Diodes with Homogeneous Multilayer Graphene Electrodes. *Appl. Phys. Express* **2013**, *6*, 072102.

(30) Jo, G.; Choe, M.; Cho, C. Y.; Kim, J. H.; Park, W.; Lee, S.; Hong, W.-K.; Kim, T.-W.; Park, S.-J.; Hong, B. H.; et al. Large-Scale Patterned Multi-Layer Graphene Films as Transparent Conducting Electrodes for GaN Light-Emitting Diodes. *Nanotechnology* **2010**, *21*, 175201.

(31) Fu, B.; Cheng, Y.; Si, Z.; Wei, T.; Zeng, X.; Yuan, G.; Liu, Z.; Lu, H.; Yi, X.; Li, J.; et al.

Phosphor-Free InGaN Micro-Pyramid White Light Emitting Diodes with Multilayer Graphene Electrode. *RSC Adv.* **2015**, *5*, 100646–100650.

(32) Bonaccorso, F.; Sun, Z.; Hasan, T.; Ferrari, A. C. Graphene Photonics and Optoelectronics. *Nat. Photonics* **2010**, *4* (9), 611–622.

(33) Suk, J. W.; Kitt, A.; Magnuson, C. W.; Hao, Y.; Ahmed, S.; An, J.; Swan, A. K.; Goldberg, B. B.; Ruoff, R. S. Transfer of CVD-Grown Monolayer Graphene onto Arbitrary Substrates. *ACS Nano* **2011**, *5* (9), 6916–6924.

(34) Zhou, L.; Epler, J. E.; Krames, M. R.; Goetz, W.; Gherasimova, M.; Ren, Z.; Han, J.; Kneissl, M.; Johnson, N. M. Vertical Injection Thin-Film AlGaN/AlGaN Multiple-Quantum-Well Deep Ultraviolet Light-Emitting Diodes. *Appl. Phys. Lett.* **2006**, *89*, 241113.

(35) Kawasaki, K.; Koike, C.; Aoyagi, Y.; Takeuchi, M. Vertical AlGaN Deep Ultraviolet Light Emitting Diode Emitting at 322 Nm Fabricated by the Laser Lift-off Technique. *Appl. Phys. Lett.* **2006**, *89*, 261114.

(36) Adivarahan, V.; Heidari, A.; Zhang, B.; Fareed, Q.; Islam, M.; Hwang, S.; Balakrishnan, K.; Khan, A. Vertical Injection Thin Film Deep Ultraviolet Light Emitting Diodes with AlGaN Multiple-Quantum Wells Active Region. *Appl. Phys. Express* **2009**, *2*, 092102.

(37) Zheng, J.-J.; Lin, Y.-J. Tuning the Work Function of Graphene by Nitrogen Plasma Treatment with Different Radio-Frequency Powers. *Appl. Phys. Lett.* **2014**, *104*, 233103.

(38) Gohda, Y.; Tsuneyuki, S. Structural Phase Transition of Graphene Caused by GaN Epitaxy. *Appl. Phys. Lett.* **2012**, *100*, 053111.

(39) Sekiguchi, H.; Kato, K.; Tanaka, J.; Kikuchi, A.; Kishino, K. Ultraviolet GaN-Based Nanocolumn Light-Emitting Diodes Grown on n-(111) Si Substrates by Rf-Plasma-Assisted Molecular Beam Epitaxy. *Phys. Status Solidi Appl. Mater. Sci.* **2008**, *205* (5), 1067–1069.

(40) Zhao, S.; Woo, S. Y.; Sadaf, S. M.; Wu, Y.; Pofelski, A.; Laleyan, D. A.; Rashid, R. T.; Wang, Y.; Botton, G. A.; Mi, Z. Molecular Beam Epitaxy Growth of Al-Rich AlGaN Nanowires for Deep Ultraviolet Optoelectronics. *APL Mater.* **2016**, *4*, 086115.

(41) Liudi Mulyo, A.; Konno, Y.; Nilsen, J. S.; Helvoort, A. T. J. Van; Fimland, B.; Weman, H.; Kishino, K. Growth Study of Self-Assembled GaN Nanocolumns on Silica Glass by Plasma Assisted Molecular Beam Epitaxy. *J. Cryst. Growth* **2017**, *480*, 67–73.

(42) Pierret, A.; Bougerol, C.; den Hertog, M.; Gayral, B.; Kociak, M.; Renevier, H.; Daudin, B. Structural and Optical Properties of $Al_xGa_{1-x}N$ Nanowires. *Rapid Res. Lett.* **2013**, *7* (10), 868–873.

(43) Pierret, A.; Bougerol, C.; Murcia-Mascaros, S.; Cros, A.; Renevier, H.; Gayral, B.; Daudin, B. Growth, Structural and Optical Properties of AlGaN Nanowires in the Whole Composition Range. *Nanotechnology* **2013**, *24*, 115704.

(44) Fernández-Garrido, S.; Koblmüller, G.; Calleja, E.; Speck, J. S. In Situ GaN Decomposition Analysis by Quadrupole Mass Spectrometry and Reflection High-Energy Electron Diffraction. *J. Appl. Phys.* **2008**, *104*, 033541.

(45) Li, L. K.; Jurkovic, M. J.; Wang, W. I.; Hove, J. M. Van; Chow, P. P. Surface Polarity Dependence of Mg Doping in GaN Grown by Molecular-Beam Epitaxy Surface. *Appl. Phys. Lett.* **2000**, *76* (13), 1740.

(46) Wu, B.; Tuncer, H. M.; Katsounaros, A.; Wu, W.; Cole, M. T.; Ying, K.; Zhang, L.; Milne, W. I.; Hao, Y. Microwave Absorption and Radiation from Large-Area Multilayer CVD Graphene. *Carbon N. Y.* **2014**, *77*, 814–822.

(47) Sarau, G.; Heilmann, M.; Bashouti, M.; Latzel, M.; Tessarek, C.; Christiansen, S. Efficient Nitrogen Doping of Single-Layer Graphene Accompanied by Negligible Defect Generation for Integration into Hybrid Semiconductor Heterostructures. *ACS Appl. Mater. Interfaces* **2017**, *9*, 10003–10011.

(48) Lee, J. E.; Ahn, G.; Shim, J.; Lee, Y. S.; Ryu, S. Optical Separation of Mechanical Strain from Charge Doping in Graphene. *Nat. Commun.* **2012**, *3* (May), 1024.

(49) Gahoi, A.; Wagner, S.; Bablich, A.; Kataria, S.; Passi, V.; Lemme, M. C. Contact Resistance Study of Various Metal Electrodes with CVD Graphene. *Solid. State. Electron.* **2016**, *125*, 234–239.

(50) Le, B. H.; Zhao, S.; Liu, X.; Woo, S. Y.; Botton, G. A.; Mi, Z. Controlled Coalescence of AlGaN Nanowire Arrays: An Architecture for Nearly Dislocation-Free Planar Ultraviolet

Photonic Device Applications. *Adv. Mater.* **2016**, *28*, 8446–8454.

(51) Qi, M.; Nomoto, K.; Zhu, M.; Hu, Z.; Zhao, Y.; Protasenko, V.; Song, B.; Yan, X.; Li, G.; Verma, J.; et al. High Breakdown Single-Crystal GaN p-n Diodes by Molecular Beam Epitaxy. *Appl. Phys. Lett.* **2015**, *107*, 232101.

(52) Pelá, R. R.; Caetano, C.; Marques, M.; Ferreira, L. G.; Furthmüller, J.; Teles, L. K. Accurate Band Gaps of AlGaN, InGaN, and AlInN Alloys Calculations Based on LDA-1/2 Approach. *Appl. Phys. Lett.* **2011**, *98*, 151907.

(53) Reshchikov, M. A.; Morkoç, H. Luminescence Properties of Defects in GaN. *J. Appl. Phys.* **2005**, *97*, 061301.

(54) Watanabe, S.; Yamada, N.; Nagashima, M.; Ueki, Y.; Sasaki, C.; Yamada, Y.; Taguchi, T.; Tadatomo, K.; Okagawa, H.; Kudo, H. Internal Quantum Efficiency of Highly-Efficient $In_xGa_{1-x}N$-Based near-Ultraviolet Light-Emitting Diodes. *Appl. Phys. Lett.* **2003**, *83* (24), 4906–4908.

(55) Wang, Q.; Connie, A. T.; Nguyen, H. P. T.; Kibria, M. G.; Zhao, S.; Sharif, S.; Shih, I.; Mi, Z. Highly Efficient, Spectrally Pure 340 Nm Ultraviolet Emission from $Al_xGa_{1−x}N$ Nanowire Based Light Emitting Diodes. *Nanotechnology* **2013**, *24* (34), 345201.

(56) Lee, I.; Choi, I.; Lee, C. R.; Noh, S. K. Evolution of Stress Relaxation and Yellow Luminescence in GaN/Sapphire by Si Incorporation. *Appl. Phys. Lett.* **1997**, *71*, 1359.

(57) Sun, W.; Shatalov, M.; Deng, J.; Hu, X.; Yang, J.; Lunev, A.; Bilenko, Y.; Shur, M.; Gaska, R. Efficiency Droop in 245-247 Nm AlGaN Light-Emitting Diodes with Continuous Wave 2 MW Output Power. *Appl. Phys. Lett.* **2010**, *96*, 061102.

(58) Muth, J. F.; Lee, J. H.; Shmagin, I. K.; Kolbas, R. M. Absorption Coefficient, Energy Gap, Exciton Binding Energy, and Recombination Lifetime of GaN Obtained from Transmission Measurements. *Appl. Phys. Lett.* **1997**, *71* (18), 2572.

(59) Djavid, M.; Mi, Z. Enhancing the Light Extraction Efficiency of AlGaN Deep Ultraviolet Light Emitting Diodes by Using Nanowire Structures. *Appl. Phys. Lett.* **2016**, *108*, 051102.

(60) Munshi, A. M.; Kim, D.-C.; Heimdal, C. P.; Heilmann, M.; Christiansen, S. H.; Vullum, P. E.; Helvoort, A. T. J. van; Weman, H. Selective Area Growth of AlGaN Nanopyramid

Arrays on Graphene by Metal-Organic Vapor Phase Epitaxy. *Appl. Phys. Lett.* **2018**, *113*, 263102.

(61) Kishino, K.; Ishizawa, S. Spectrally-Broadened Multimode Lasing Based on Structurally Graded InGaN Nanocolumn Photonic Crystals Suitable for Reduction of Speckle Contrast. *Appl. Phys. Lett.* **2016**, *109*, 071106.

(62) Yamano, K.; Kishino, K. Selective Area Growth of InGaN-Based Nanocolumn LED Crystals on AlN/Si Substrates Useful for Integrated μ-LED Fabrication. *Appl. Phys. Lett.* **2018**, *112*, 091105.

(63) Nguyen, H. P. T.; Cui, K.; Zhang, S.; Djavid, M.; Korinek, A.; Botton, G. A.; Mi, Z. Controlling Electron Overflow in Phosphor-Free InGaN/GaN Nanowire White Light-Emitting Diodes. *Nano Lett.* **2012**, *12* (3), 1317–1323.

(64) Han, J.; Crawford, M. H.; Shul, R. J.; Figiel, J. J.; Banas, M.; Zhang, L.; Song, Y. K.; Zhou, H.; Nurmikko, A. V. AlGaN/GaN Quantum Well Ultraviolet Light Emitting Diodes. *Appl. Phys. Lett.* **1998**, *73*, 1688–1690.

(65) Wang, L.; Liu, W.; Zhang, Y.; Zhang, Z.-H.; Tan, S. T.; Yi, X.; Wang, G.; Sun, X.; Zhu, H.; Demir, H. V. Graphene-Based Transparent Conductive Electrodes for GaN-Based Light Emitting Diodes: Challenges and Countermeasures. *Nano Energy* **2015**, *12*, 419–436.

(66) Li, Z.; Kang, J.; Liu, Z.; Du, C.; Lee, X.; Li, X.; Wang, L.; Yi, X.; Zhu, H.; Wang, G. Enhanced Performance of GaN-Based Light-Emitting Diodes with Graphene/Ag Nanowires Hybrid Films. *AIP Adv.* **2013**, *3*, 042134.

(67) Choe, M.; Cho, C.-Y.; Shim, J.-P.; Park, W.; Lim, S. K.; Hong, W.-K.; Lee, B. H.; Lee, D.-S.; Park, S.-J.; Lee, T. Au Nanoparticle-Decorated Graphene Electrodes for GaN-Based Optoelectronic Devices. *Appl. Phys. Lett.* **2012**, *101*, 031115.